Applied Surface Science 742 (2026) 167187

Contents lists available at ScienceDirect

Applied Surface Science

journal homepage: www.elsevier.com/locate/apsusc

Full length article

Kapitza resistance and thermal transport in knotted graphene nanoribbons

Levi C. Felix [a], Marcelo L. Pereira Junior [b,*], Guilherme S.L. Fabris [a], Alexandre F. Fonseca [a], Douglas S. Galvão [a,c]

[a] Universidade Estadual de Campinas, Instituto de Física Gleb Wataghin, Departamento de Física Aplicada, 13083-859, Campinas, SP, Brazil
[b] University of Brasília, College of Technology, Department of Electrical Engineering, 70910-900, Brasília, DF, Brazil
[c] Department of Applied Physics, State University of Campinas, Campinas, SP, 13083-970, Brazil

ARTICLE INFO

Keywords:
Graphene nanoribbons
Kapitza resistance
Thermal transport
Phonon scattering
Non-equilibrium molecular dynamics

ABSTRACT

Thermal transport in low-dimensional systems is central to nanoscale heat dissipation and phonon engineering applications, particularly in materials where geometry and structural distortions strongly influence scattering mechanisms. In this context, graphene nanoribbons constitute a well-defined platform for investigating thermal transport due to their quasi-one-dimensional character and tunable structural properties. In this work, we have investigated the effect of structural knots on the thermal transport of graphene nanoribbons using non-equilibrium molecular dynamics simulations (NEMD). Systems containing one, two, and three knots were considered. The temperature profiles exhibit localized temperature drops at the knot positions, indicating the emergence of thermal resistance in these regions. This behavior is analogous to Kapitza resistance observed at interfaces between dissimilar materials or in single materials containing defects or lattice distortions. The thermal resistance associated with an individual knot is approximately constant. The total thermal resistance increases almost linearly with the number of knots, consistent with a series arrangement of thermal resistances. In addition, variations in the relative positions of the knots along the nanoribbon do not significantly affect the heat current driven by the imposed temperature gradient, indicating a weak thermal rectification effect for the configurations investigated.

1. Introduction

Graphene nanoribbons (GNRs) have been of interest to the materials physics community since they belong to one-dimensional systems and possess a very simple structure, being actually narrow-striped graphene sheets. Their electronic features are largely determined by the edge type, that is either armchair or zigzag [1–4], giving rise to localized edgestates in zigzag GNRs but not in armchair ones. Very recently, topological phases driven by external electric field and boron or nitrogen doping have been found [5], which further substantiates the interest in GNRs for potential applications in quantum electronics [6]. In this respect, heat transport is a critical process as the hot and cold cycles are constantly experienced by electronic devices. In low-dimensional systems, thermal conduction is largely controlled by surface roughness, where most of the phonon scattering mechanisms take place [7,8]. However, for GNRs the mean free path of most dominant phonon modes (∼ 1 nm) greatly exceeds the typical height fluctuations at the surface (0.2–0.6 Å) [9]), meaning that other phonon scattering mechanisms can be relevant in heat conduction. The successful experimental realization of GNRs [10–12] has made the systematic studies on their electronic structure [13] and heat transport properties [14] feasible, which opens an avenue for a controlled study of phonon thermal transport in quasi-one-dimensional carbon-based systems.

Defect engineering has emerged as an effective strategy to tailor the physical properties of GNRs beyond those of pristine structures. Representative examples include spin filtering effects induced by the combination of vacancies and boron or nitrogen doping [15], as well as bandgap tuning achieved through edge patterning mediated by vacancy defects [16]. Beyond point and edge defects, geometrical distortions have been explored as an additional degree of freedom to modulate the properties of GNRs. Twisted nanoribbons have been theoretically investigated [17,18], with helical configurations shown to be energetically more favorable than simple torsional deformations. In a recent work, the thermal conductivity of twisted GNRs was shown to depend not solely on the number of initial turns applied to the GNR, but also on the twist density along its length [19]. The degree of twisting has also been shown to affect the charge-carrier type and mobility [20]. Further studies have reported conformationally dependent properties [21], nonlinear current–voltage characteristics under transverse electric fields [22], mechanical strengthening when GNRs are

* Corresponding author.
E-mail address: marcelo.lopes@unb.br (M.L. Pereira Junior).

https://doi.org/10.1016/j.apsusc.2026.167187
Received 26 February 2026; Received in revised form 17 April 2026; Accepted 9 May 2026
Available online 15 May 2026

confined inside carbon nanotubes [23], and even chirality-controlled carbon nanotube synthesis [24].

Knots constitute another kind of geometrical structures with a number of investigations in a diversity of carbon-based and fibrous materials such as carbon-nanotubes [25], polymer and nanotube microfibers [26,27], graphene oxide fibers [28] silk-fibers [29] and graphene nanoribbons [30]. In the GNR context, these metastable states are known to have been found more than one for a given knotted configuration under different tension conditions, and spin-polarized solutions of the electronic ground state can be found in tightly knotted configurations; such properties have been associated with local structural reconstruction contributing to an enhancement of electronic localization. The mechanical response of knotted nanostructures has been reviewed in detailed studies [25–30], but the disruption of local topology effect on heat conduction is less studied. This missing information is rather crucial because knots generate strong local curvature, strain fields, and lattice inhomogeneities, which are thought to significantly influence the phonon scattering processes and thermal resistance.

In the present paper, we have investigated the effect of knotted graphene nanoribbons on thermal transport via Non-Equilibrium Molecular Dynamics (NEMD) simulations. We have considered systems with one, two, and three knots in the presence of a temperature gradient established by thermal reservoirs at different temperatures. For a direct comparison, we have also considered the pristine nanoribbons without knots or twists to explicitly determine the effects of knotted geometric deformations on heat flux and the appearance of Kapitza thermal resistance [31,32] in graphene nanoribbons.

2. Methods

To create the knotted GNRs, we initially generated straight hydrogen-passivated nanoribbon structures with width $W = 10$ Å using the Visual Molecular Dynamics (VMD) software [33]. Crucially, the hydrogen passivation of the nanoribbon edges was implemented specifically to avoid any unintended rehybridization or bond reconstruction. This ensures that all carbon atoms remain 3-fold coordinated, allowing us to isolate the effects of local topology and curvature on thermal transport without the interference of changes in the local bonding state. A pre-knotted geometry was then obtained by mapping the nanoribbon onto four control points using the sculptor tool. Fig. 1 shows four representative structural stages observed during the knot formation process. Stage (1) corresponds to the initial pre-knotted configuration. Stages (2) and (3) illustrate intermediate geometries obtained during the progressive tightening of the knot under uniaxial stretching. Stage (4) shows the final tightly closed and structurally relaxed knotted configuration.

The same creating procedure was repeated to generate GNRs containing two and three knots, as shown at the bottom of Fig. 1. In these configurations, the distance between neighboring knots was fixed at $d = 60$ Å, and the total length of the GNRs was $L = 30$ nm. For comparison purposes, pristine (knotless) GNRs with identical lengths were also considered.

All GNRs were modeled as suspended structures with both ends fixed, as illustrated in Fig. 2. Thermal transport properties were investigated using classical molecular dynamics simulations performed with the LAMMPS package [34]. Prior to the NEMD simulations, all systems were thermally equilibrated in an NVT ensemble for 100 ps to ensure structural relaxation and thermal stability.

Interatomic interactions among all atoms were described using the adaptive intermolecular reactive empirical bond order (AIREBO) potential, which allows for a consistent treatment of C–C, C-H, and H-H interactions within a single framework [35]. This choice ensures an accurate description of both the covalent backbone of the graphene nanoribbons and the hydrogen-passivated edges, while properly accounting for bond

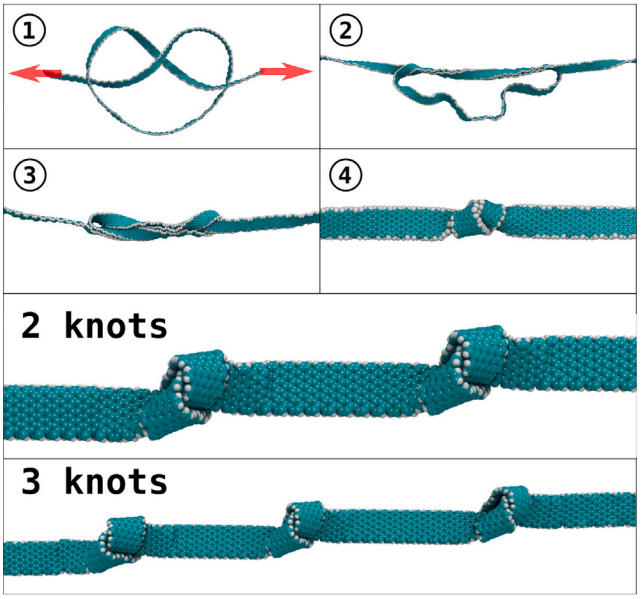

Fig. 1. Representative structural stages of the GNR knot formation process. Panels (1)-(4) show successive configurations obtained during the tightening of a single knot, from the initial pre-knotted geometry to the final tightly closed and relaxed configuration. The bottom panels show GNRs with two and three knots, respectively. Carbon and hydrogen atoms are shown in green and white, respectively.

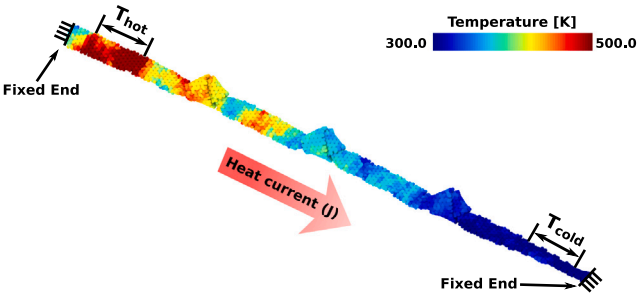

Fig. 2. Simulation setup used to generate a temperature gradient in a knotted GNR. Both ends of the nanoribbon are fixed, while hot and cold thermostatted regions are applied near the ends. Atoms are colored according to their spatially averaged atomic temperature.

stretching, angle bending, and nonbonded interactions [36]. Additionally, previous studies have shown that AIREBO provides the most accurate predictions of vibrational properties of highly curved carbon structures relative to first-principles calculations when compared to other force fields [37]. After the equilibration stage, the atoms at both ends of the GNRs were fixed to define the suspended configuration used in the thermal transport simulations.

To create a temperature gradient, two Nosé–Hoover thermostatted regions with lengths of 40 Å were defined near the fixed ends of the GNRs, as shown in Fig. 2. These regions acted as thermal reservoirs maintained at temperatures $T_{hot} = 500$ K and $T_{cold} = 300$ K, generating a heat current flowing from the hot to the cold bath. The temperature gradient was established by integrating the equations of motion using an NVT ensemble in the thermostatted regions and an NVE ensemble for the atoms located between the two reservoirs for 1 ns. This procedure allowed the system to reach a steady state in which the energy entering the cold reservoir balances the energy leaving the hot reservoir. A similar NEMD methodology has been shown to agree well with experimentally obtained results for pristine graphene [38,39].

Fig. 2 presents an example of the spatial temperature distribution obtained for a GNR containing three knots. Once the system reaches the stationary regime, characterized by a constant heat flux, the temperature profile is obtained by dividing the nanoribbon into slabs along the transport direction. The temperature of each slab is computed from the average kinetic energy of the atoms belonging to that slab, according to the equipartition theorem [40–42]:

$$T_i = \frac{1}{3N_i k_B} \sum_{j=1}^{N_i} \frac{p_j^2}{m_j}, \tag{1}$$

where T_i is the temperature of the ith slab, N_i is the number of atoms in the slab, k_B is the Boltzmann constant, and m_j and p_j are the mass and linear momentum of atom j, respectively. This slab-based definition provides a physically meaningful description of the local temperature under non-equilibrium conditions. It ensures that the resulting temperature profile reproduces the macroscopic temperature gradient imposed by the thermal reservoirs. In Fig. 2, the color map represents the slab-averaged temperatures, obtained by spatial averaging over neighboring atoms within a cutoff radius of 5 Å, as implemented in the OVITO software [43]. After establishing the steady-state thermal gradient, additional MD simulations of 1 ns were performed to compute the temperature profile and to monitor the cumulative energy exchanged with the hot and cold reservoirs.

The heat current J was obtained from the slope of the cumulative energy exchanged with the reservoirs as a function of time. Using the one-dimensional form of Fourier's law of heat conduction, the heat flux q is given by

$$q = \frac{J}{A} = \kappa \frac{dT}{dx}, \tag{2}$$

where A is the effective cross-sectional area defined as $A = (W \times 3.35)$ Å^2, with 3.35 Å corresponding to the conventionally assumed thickness of a graphene monolayer, dT/dx is the temperature gradient, and κ is the thermal conductivity.

Local discontinuities ΔT in the temperature profile are indicative of thermal resistances (R). This concept is commonly used to describe heat transport across interfaces between different materials, defining the so-called Kapitza resistance [44], which is expressed as:

$$R = \frac{\Delta T}{q}. \tag{3}$$

Although originally introduced for heterogeneous interfaces, Kapitza-like thermal resistances have also been reported in systems composed of a single material in the presence of defects [45–48] and lattice distortions [49–53].

3. Results

We will first discuss the steady-state temperature profiles along GNRs with 0, 1, 2, and 3 knots under a thermal gradient. This result enables us to directly determine the impact of localized geometrical distortions on the inhomogeneity of spatial temperature distribution and changes in the heat-transport mechanism across the nanoribbon. In the current study, it is shown that the presence of knots facilitates the distinction of local temperature discontinuities and provides a meaningful way to interpret knots as additional scattering centers for phonons. From these profiles we then calculate the heat current-response and obtain the thermal resistance of individual knots, focusing on whether and how this resistive contribution changes with increasing number of knots.

The temperature profiles of GNRs without knots and with one, two, and three knots are presented in Fig. 3. Flat regions and knot positions were distinguished by mapping the physical location of the knots directly onto the temperature profile, where the x-coordinate represents the center of the spatial blocks (bins) used to calculate the local temperature. For all cases, we performed three independent NEMD simulations and reported error bars for each spatial bin in which the local temperature is computed. In all cases, the red lines indicate flat regions of the nanoribbons in which the temperature varies approximately linearly with position, and the temperature gradient dT/dx remains nearly constant. The green lines correspond to the regions where knots are located and where deviations from this linear behavior are observed. For the pristine GNR shown in Fig. 3(a), a well-defined linear temperature profile is obtained along most of the nanoribbon length, indicating diffusive heat transport. Nonlinear variations appear only near the thermal baths, where the temperature changes more rapidly due to phonon scattering at the interfaces between thermostatted and non-thermostatted regions, a behavior commonly observed in NEMD simulations [54–56].

In contrast, the temperature profiles of GNRs containing 1, 2, and 3 knots, shown in Figs. 3(b–d), exhibit clear temperature drops at the positions of the knots. Each knot introduces a localized discontinuity ΔT in the temperature profile, accompanied by a change in the local temperature gradient relative to the flat regions. These features indicate that the knots act as localized thermal resistances, where additional phonon scattering induced by the geometric distortion reduces the effective heat transport. As the number of knots increases, multiple temperature drops appear along the nanoribbon, each associated with a distinct knot, demonstrating that the overall thermal resistance increases through the successive addition of these localized resistive elements.

To determine the thermal conductivity κ of the system, we first evaluate the heat flux q generated in the NEMD simulations. This is achieved by monitoring the time evolution of the cumulative energy exchanged with the hot and cold reservoirs. The heat current J is obtained from the slope of the linear fits to these cumulative energy curves, as illustrated in Fig. 4(a) for the case of a GNR containing one knot. In this example, the slopes associated with the right and left reservoirs are 0.748 and −0.749 eV/ps, respectively, indicating that a steady-state heat flow has been established. The heat current is then computed as the arithmetic average of the absolute values of these slopes, yielding $J = (0.748 + |-0.749|)/2 \approx 0.749$ eV/ps.

Fourier's law was applied only to regions where the temperature varies linearly with position. Accordingly, the thermal conductivity of each flat or knotted segment is obtained by dividing the heat flux by the absolute value of the corresponding temperature gradient. As previously shown by the temperature profiles in Fig. 3, the knotted regions behave as segments with an effective thermal conductivity κ^k that differs from that of the flat regions. The effective thermal conductivity of the entire quasi-one-dimensional structure is therefore calculated using a series-resistance model commonly employed for layered composites [54,57], given by:

$$\frac{1}{\kappa_{\text{eff}}} = \sum_{i=1}^{N_k+1} \frac{\phi_i}{\kappa_i} + \sum_{i=1}^{N_k} \frac{\phi_i^k}{\kappa_i^k}, \tag{4}$$

where N_k is the number of knots, $\phi_i = l_i/L_x$ and $\phi_i^k = l_i^k/L_x$ are the length fractions of the flat and knotted regions, respectively, and κ_i and κ_i^k are their corresponding thermal conductivities.

Each κ_i is obtained as:

$$\kappa_i = q \left(\left| \frac{dT}{dx} \right|_i \right)^{-1}, \tag{5}$$

with q being the heat flux along the nanoribbon and $|dT/dx|_i$ the slope of the temperature gradient in the region i. An analogous expression applies to the knotted regions.

The dependence of both the heat current J and the effective thermal conductivity κ_{eff} on the number of knots is shown in Fig. 4(b). For the pristine GNR, the heat current is approximately 0.75 eV/ps and the effective thermal conductivity is close to 75 W/mK. The introduction of a single knot leads to a marked decrease of both quantities, with J decreasing to about 0.50 eV/ps and κ_{eff} to roughly 50 W/mK. When two knots are present, the heat current is further reduced to approximately 0.43 eV/ps, while κ_{eff} drops to around 32 W/mK. For three knots, J

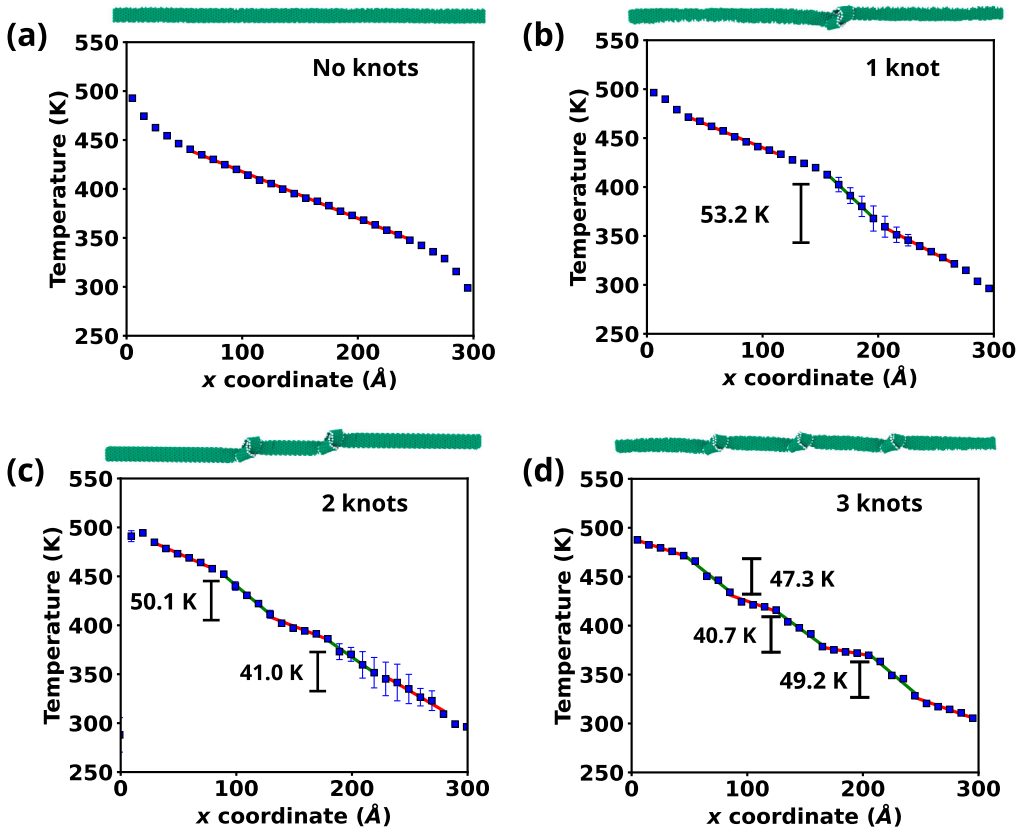

Fig. 3. Temperature profiles of GNRs with (a) zero, (b) one, (c) two, and (d) three knots. Red lines correspond to linear regressions performed in flat regions without knots, and green lines indicate the fitted temperature gradients within the knot regions.

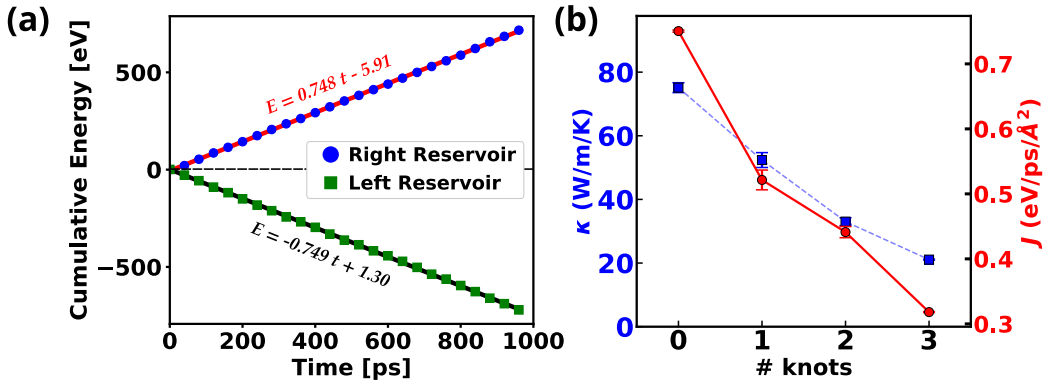

Fig. 4. Heat current and effective thermal conductivity. (a) Time evolution of the cumulative energy exchanged with the hot and cold reservoirs and their corresponding linear fits. (b) Dependence of the heat current J and the effective thermal conductivity κ_{eff} on the number of knots.

reaches values close to 0.32 eV/ps and κ_{eff} decreases to about 22 W/mK. This monotonic decay indicates that each additional knot contributes to an extra thermal resistance, progressively suppressing heat transport as the number of knots increases.

With the heat flux obtained for all cases, we can calculate the Kapitza resistance induced by the presence of knots in the GNRs. Table 1 shows the temperature drops ΔT associated with each knot for nanoribbons containing 1, 2, and 3 knots, now averaged over independent runs with associated statistical uncertainties. In the single-knot configuration, a temperature discontinuity of $\Delta T = 53.2 \pm 8.0$ K is observed. For two knots, the temperature drops to 50.1 ± 3.2 and 41.0 ± 16.8 K, indicating a reduction relative to the single-knot case, although the second knot exhibits a relatively large statistical uncertainty. When three knots are present, ΔT further decreases to values between 40.7 ± 1.3 and 49.2 ± 0.7 K, confirming a systematic reduction in the temperature discontinuity as additional knots are introduced. Despite this decrease, the corresponding Kapitza resistances remain of the same order of magnitude. The resistance is $2.14 \pm 0.34 \times 10^{-10}$ m^{2}K/W for one knot, 2.38 ± 0.19 and $1.96 \pm 0.82 \times 10^{-10}$ m^{2}K/W for two knots, and values between 2.67 ± 0.01 and $3.23 \pm 0.04 \times 10^{-10}$ m^{2}K/W for three knots. Within the statistical uncertainties, the single- and two-knot cases are consistent with each other, while the three-knot configuration shows a tendency toward slightly higher resistance values. This behavior reflects the proportional reduction of the heat flux q (and correspondingly J) as additional knots are introduced, keeping the ratio $\Delta T/q$ approximately constant for each knot within uncertainty. Consequently, each knot contributes an approximately similar thermal resistance, and the total thermal resistance of nanoribbons containing

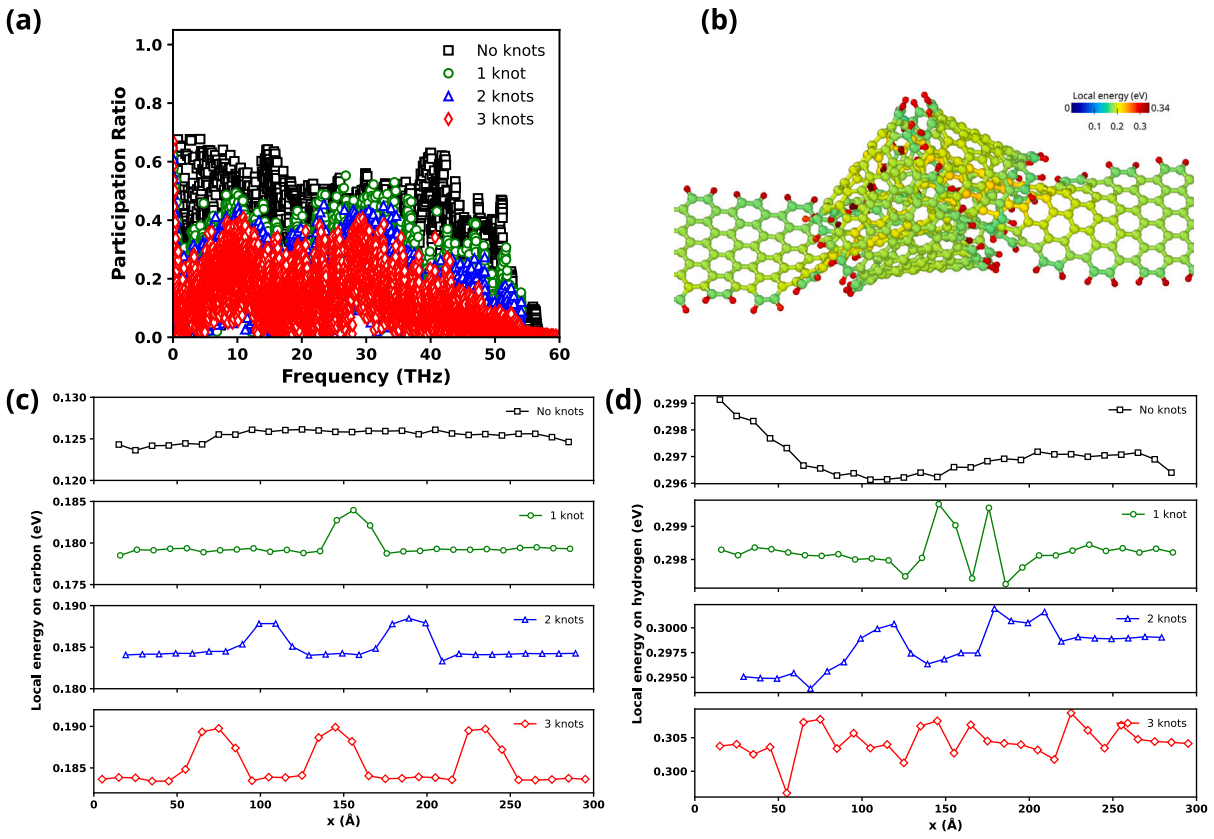

Fig. 5. (a) Participation ratio as a function of frequency for graphene nanoribbons with no knots and with one, two, and three knots. (b) Spatial distribution of the localized vibrational energy for a representative knotted configuration at 300 K. (c) Longitudinal profile of the local energy projected onto carbon atoms for different knot configurations. (d) Longitudinal profile of the local energy projected onto hydrogen atoms for different knot configurations.

Table 1
Temperature drops ΔT and the corresponding interfacial Kapitza thermal resistances R induced by each knot for GNRs with one, two, and three knots.

Number of knots	ΔT [K]	R [10^{-10}m^2/W K]
1	53.2 ± 8.0	2.14 ± 0.34
2	50.1 ± 3.2	2.38 ± 0.19
	41.0 ± 16.8	1.96 ± 0.82
3	47.3 ± 2.9	3.11 ± 0.19
	40.7 ± 1.3	2.67 ± 0.01
	49.2 ± 0.7	3.23 ± 0.04

two and three knots remains consistent with a series association of localized thermal resistances, with possible deviations emerging only in the three-knot configuration due to increased knot–knot interactions.

To further elucidate the microscopic origin of heat transport in knotted graphene nanoribbons, we analyze phonon localization through the participation ratio (PR) and the corresponding spatial distribution of vibrational energy. The participation ratio for a phonon mode λ is defined as

$$P_\lambda = \frac{1}{N \sum_i \left(\sum_\alpha |\varepsilon_{i\alpha,\lambda}|^2 \right)^2}, \tag{6}$$

where N is the total number of atoms, $\varepsilon_{i\alpha,\lambda}$ is the α-th Cartesian component ($\alpha = x, y, z$) of the eigenvector of mode λ at atom i. The PR quantifies the degree of localization of a phonon mode, with values close to unity corresponding to extended modes and small values indicating spatially localized vibrations. To visualize where these localized modes reside in real space, we compute the local vibrational energy

$$E_i = \sum_{\lambda,\, P_\lambda < 0.4} \left(n_\lambda + \frac{1}{2} \right) \hbar \omega_\lambda \sum_\alpha |\varepsilon_{i\alpha,\lambda}|^2, \tag{7}$$

with ω_λ is the angular frequency of mode λ, $\hbar$ is the reduced Planck constant, and $n_\lambda = [\exp(\hbar\omega_\lambda / k_B T) - 1]^{-1}$ is the Bose–Einstein occupation factor at temperature T. The summation is restricted to modes with $P_\lambda < 0.4$ to isolate spatially localized phonons, as commonly adopted in the literature [58], thereby highlighting regions where vibrational energy is confined and which are most relevant to phonon scattering and thermal resistance.

Fig. 5(a) shows the participation ratio (PR) as a function of frequency for graphene nanoribbons with different numbers of knots, where the overall reduction in PR with increasing knot number indicates an enhanced presence of localized phonon modes. The spatial distribution of the corresponding localized vibrational energy is illustrated in Fig. 5(b), where higher intensity colors are clearly concentrated within the knot region for both carbon and hydrogen atoms, confirming that knots act as strong phonon localization centers. Although the overall magnitude of the local energy is higher on the edge due to passivating hydrogen atoms, an enhancement within the knot is observed for both atomic species, indicating that the knot geometry amplifies vibrational localization beyond the intrinsic edge effect.

To further quantify this behavior, Figs. 5(c) and (d) present the longitudinal profiles of the local energy projected onto carbon and hydrogen atoms, respectively. The carbon atoms exhibit pronounced localization peaks in the vicinity of the knots, directly reflecting the role of the carbon backbone in longitudinal heat transport. In contrast,

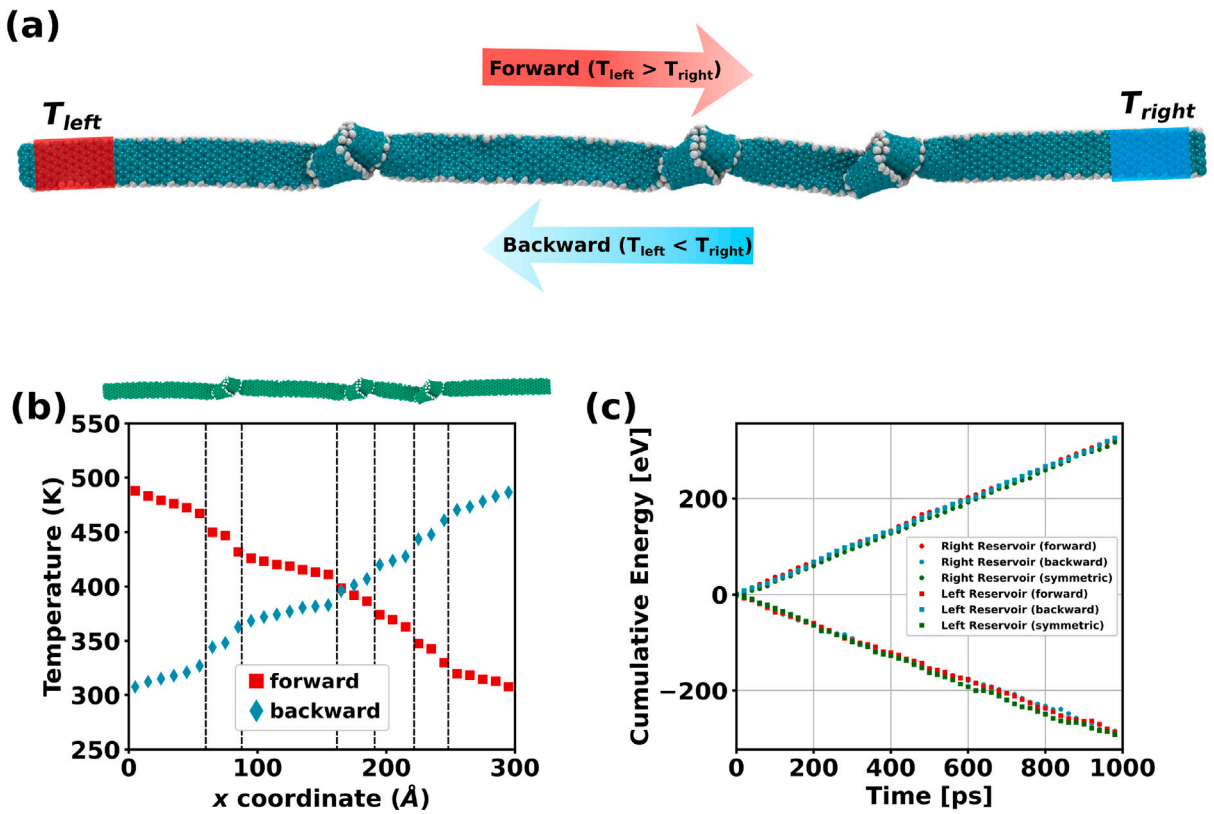

Fig. 6. Thermal transport in asymmetrically three-knot GNRs. (a) Simulation setup illustrating the asymmetric knot arrangement and the definition of forward and backward heat transport. (b) Temperature profiles for forward and backward configurations. (c) Time evolution of the cumulative energy exchanged with the hot and cold reservoirs for forward, backward, and symmetric configurations.

hydrogen atoms display larger absolute values due to their lighter mass and high-frequency vibrational character, while still showing an overall increase in the knot regions. These results indicate that, although edge hydrogen atoms dominate the magnitude of the local energy, the knot-induced localization is a collective effect involving both carbon and hydrogen atoms, with longitudinal thermal transport primarily governed by the carbon network.

In the two-knot system, the localized energy becomes more strongly concentrated within each knot region for both atomic species. In contrast, in the three-knot configuration, the spatial distribution of the localized energy along the edge remains relatively extended along the ribbon, suggesting that the vibrational response is not fully confined to individual knots. This inhibited confinement indicates that the presence of additional knots promotes stronger phonon localization, thereby increasing scattering and reducing the ability of vibrational modes to propagate along the ribbon. This provides a possible explanation for why the resistance remains similar from one to two knots but increases in the three-knot configuration, despite identical knot spacing.

Lastly, we have also investigated the thermal transport in a knotted GNR with an asymmetric knot arrangement to assess the potential emergence of thermal rectification effects. This analysis is motivated by previous studies reporting rectification in geometrically asymmetric graphene and MoS_2 nanoribbons, where reversing the temperature bias leads to different heat fluxes [45,46,59–62]. In the present case, asymmetry is introduced by displacing one of the knots relative to the others, as illustrated in Fig. 6(a), where the first two knots are separated by 100 Å and the third knot is placed 50 Å away from the second one. Two thermostatted regions are applied near the fixed ends of the nanoribbon at temperatures T_{left} and T_{right}, defining forward heat transport when $T_{left} > T_{right}$ and backward transport when $T_{left} < T_{right}$.

The temperature profiles corresponding to the forward and backward configurations are shown in Fig. 6(b). The backward profile is essentially a mirror inversion of the forward one, indicating that the local temperature gradients and temperature drops at the knot positions are nearly identical upon reversing the thermal bias. This symmetry is further reflected in the cumulative energy curves displayed in Fig. 6(c), where the total energy exchanged with the reservoirs after 1 ns differs by approximately 0.7% between forward and backward cases. This difference is comparable to the uncertainty associated with reaching the steady state, estimated to be about 0.5%, indicating that the heat currents in both directions are effectively the same within numerical accuracy.

To quantify the rectification effect, we computed the rectification factor:

$$\eta = \frac{q_f}{q_b} - 1, \tag{8}$$

where q_f and q_b are the heat fluxes in the forward and backward directions, respectively. For the asymmetrically knotted GNR considered here, we obtained $\eta \approx 0.3\%$. This value is significantly smaller than rectification factors reported for other asymmetric graphene and MoS_2 nanoribbons, which typically range from 1% up to 25% in NEMD simulations [45,46,60]. Therefore, despite the geometric asymmetry introduced by the displaced knot, the resulting rectification remains too weak to characterize knotted GNRs as efficient thermal diodes.

This behavior can be understood by noting that knot formation primarily induces localized strain and structural distortions that act as phonon scattering centers but do not introduce a sufficiently strong directional asymmetry in phonon transmission. As a result, although each knot contributes to thermal resistance, the overall heat transport remains largely reciprocal upon reversing the temperature bias. Effects related to size dependence, such as variations in ribbon length and width, which significantly influence thermal transport in graphene-based systems, were not addressed in the present work and will be considered in future investigations.

The atomic-level precision achieved in the bottom-up fabrication of nanoribbons with tunable topological phases [63] demonstrates that complex geometric control is already possible in carbon-based systems. Furthermore, the successful creation of intricate molecular knots in synthetic polymers [64] and the study of knot dynamics in DNA [65] highlight the growing technical ability to manipulate topology at the nanoscale. These cross-disciplinary advancements suggest that structural knots can serve as robust modulators of physical properties in low-dimensional materials. We have updated the manuscript to include these references and to discuss how these emerging techniques bridge the gap between our theoretical findings and practical implementation in 2D systems.

4. Conclusions

In conclusion, we have investigated the thermal transport in knotted GNR using NEMD, focusing on the role of geometric knots as sources of phonon scattering. The results demonstrate that each knot introduces a localized temperature discontinuity, which can be consistently interpreted as a Kapitza-like thermal resistance arising from local curvature, strain fields, and lattice distortion. Notably, the thermal resistance associated with an individual knot remains nearly constant. In contrast, the total thermal resistance increases approximately linearly with the number of knots, evidencing a series-like addition of localized resistive elements along the nanoribbon.

The presence of multiple knots leads to a systematic decrease in both the heat current and the effective thermal conductivity, with values decreasing from those of pristine ribbons to approximately one-third when three knots are introduced. Despite variations in the relative magnitude of the local temperature jumps, the corresponding Kapitza resistances remain within a narrow range, confirming that the dominant effect of additional knots is the suppression of heat flux rather than a qualitative change in the transport mechanism.

We have also analyzed an asymmetrically knotted nanoribbon to assess the possibility of an effective thermal rectification. The forward and backward transport regimes exhibit nearly identical temperature profiles and cumulative energy exchange. The resulting rectification factor remains below one percent, indicating that knot-induced asymmetry alone is insufficient to generate a pronounced non-reciprocal thermal response. This behavior highlights that, while knots act as efficient phonon scatterers, they do not break thermal reciprocity to a degree comparable to other asymmetric nanostructures reported in the literature.

Overall, these findings establish structural knots as robust and tunable modulators of thermal transport in graphene nanoribbons, enabling controlled suppression of heat conduction through purely geometric means. While the present study focused on fixed ribbon dimensions, the strong size dependence of thermal transport in graphene-based systems suggests that the interplay among knot topology, ribbon width, and length may provide additional pathways to tailor thermal functionality [19,66]. These aspects will be addressed in future investigations. Future studies may also explore alternative sources of asymmetry, such as knots with different sizes, multiple or double-knot configurations, or variations in knot tightness, which could enhance directional phonon scattering and potentially induce measurable thermal rectification. A systematic investigation of how geometric parameters such as knot size, curvature, and tightness affect the Kapitza resistance would also provide further insight into the underlying mechanisms and is an interesting direction for future work.

CRediT authorship contribution statement

Levi C. Felix: Writing – original draft, Visualization, Software, Methodology, Formal analysis, Data curation. **Guilherme S.L. Fabris:** Writing – original draft, Methodology, Formal analysis. **Alexandre F. Fonseca:** Writing – review & editing, Methodology, Investigation, Funding acquisition, Formal analysis, Conceptualization. **Douglas S. Galvão:** Writing – review & editing, Validation, Supervision, Software, Resources, Project administration, Methodology, Investigation, Formal analysis. **Marcelo L. Pereira Junior:** Writing – review & editing, Validation, Supervision, Resources, Investigation, Funding acquisition, Formal analysis.

Declaration of competing interest

The authors declare the following financial interests/personal relationships which may be considered as potential competing interests: Guilherme da Silva Lopes Fabris reports financial support was provided by State of Sao Paulo Research Foundation. Marcelo Lopes Pereira Junior reports financial support was provided by Foundation for Research Support of the Federal District. Marcelo Lopes Pereira Junior reports financial support was provided by Coordination for the improvement of Higher Education Personnel. Marcelo Lopes Pereira Junior reports financial support was provided by National Council for Scientific and Technological Development. Alexandre Fontes Fonseca reports financial support was provided by National Council for Scientific and Technological Development. Alexandre Fontes Fonseca reports financial support was provided by State of Sao Paulo Research Foundation. Douglas Soares Galvao reports financial support was provided by State of Sao Paulo Research Foundation. If there are other authors, they declare that they have no known competing financial interests or personal relationships that could have appeared to influence the work reported in this paper.

Acknowledgments

This work was supported by the São Paulo Research Foundation (FAPESP), the Federal District Research Support Foundation (FAPDF), the National Council for Scientific and Technological Development (CNPq), and the Coordination for the Improvement of Higher Education Personnel (CAPES). Computational resources were provided by the Center for Computing in Engineering and Sciences at the University of Campinas, with financial support from FAPESP through the CEPID program under Grants 2013/08293-7 and 2018/11352-7. G.S.L.F. acknowledges a fellowship from FAPESP under Process 2024/03413-9. M.L.P.J. acknowledges financial support from FAPDF under Grant No. 00193-00001807/2023-16, from CNPq under Grants 444921/2024-9 and 308222/2025-3, and from CAPES under Grant No. 88887.005164/2024-00. A.F.F. is a fellow of CNPq under Grant No. 302009/2025-6 and acknowledges support from FAPESP under Grant No. 2024/14403-4. D.S.G. acknowledges support from the National Institute of Organic Electronics (INEO), CNPq, and FAPESP under Grant No. 2025/27044-5.

Data availability

Data will be made available on request.

References

[1] Katsunori Wakabayashi, Ken-Ichi Sasaki, Takeshi Nakanishi, Toshiaki Enoki, Electronic states of graphene nanoribbons and analytical solutions, Sci. Technol. Adv. Mater. 11 (5) (2010) 054504.
[2] Young-Woo Son, Marvin L. Cohen, Steven G. Louie, Energy gaps in graphene nanoribbons., Phys. Rev. Lett. 97 (21) (2006) 216803.
[3] K. Nakada, M. Fujita, G. Dresselhaus, MS Dresselhaus, Edge state in graphene ribbons: Nanometer size effect and edge shape dependence., Phys. Rev. B, Condens. Matter 54 (24) (1996) 17954–17961.
[4] J. Jiang, W. Lu, J. Bernholc, Edge states and optical transition energies in carbon nanoribbons., Phys. Rev. Lett. 101 (24) (2008) 246803.
[5] Fangzhou Zhao, Ting Cao, Steven G. Louie, Topological phases in graphene nanoribbons tuned by electric fields., Phys. Rev. Lett. 127 (16) (2021) 166401.

[6] Haomin Wang, Hui Shan Wang, Chuanxu Ma, Lingxiu Chen, Chengxin Jiang, Chen Chen, Xiaoming Xie, An-Ping Li, Xinran Wang, Graphene nanoribbons for quantum electronics, Nat. Rev. Phys. 3 (12) (2021) 791–802.

[7] Z. Aksamija, I. Knezevic, Thermal transport in graphene nanoribbons supported on SiO, Phys. Rev. B 86 (16) (2012) 165426.

[8] Giorgia Fugallo, Luciano Colombo, Calculating lattice thermal conductivity: a synopsis, Phys. Scr. 93 (4) (2018) 043002.

[9] Yan Wang, Bo Qiu, Xiulin Ruan, Edge effect on thermal transport in graphene nanoribbons: A phonon localization mechanism beyond edge roughness scattering, Appl. Phys. Lett. 101 (1) (2012) 013101.

[10] Jinming Cai, Pascal Ruffieux, Rached Jaafar, Marco Bieri, Thomas Braun, Stephan Blankenburg, Matthias Muoth, Ari P Seitsonen, Moussa Saleh, Xinliang Feng, Klaus Müllen, Roman Fasel, Atomically precise bottom-up fabrication of graphene nanoribbons., Nature 466 (7305) (2010) 470–473.

[11] Xiaolin Li, Xinran Wang, Li Zhang, Sangwon Lee, Hongjie Dai, Chemically derived, ultrasmooth graphene nanoribbon semiconductors., Science 319 (5867) (2008) 1229–1232.

[12] Liying Jiao, Li Zhang, Xinran Wang, Georgi Diankov, Hongjie Dai, Narrow graphene nanoribbons from carbon nanotubes., Nature 458 (7240) (2009) 877–880.

[13] Xinran Wang, Yijian Ouyang, Xiaolin Li, Hailiang Wang, Jing Guo, Hongjie Dai, Room-temperature all-semiconducting sub-10-nm graphene nanoribbon field-effect transistors., Phys. Rev. Lett. 100 (20) (2008) 206803.

[14] Junjie Chen, Baofang Liu, Ballistic heat conduction characteristics of graphene nanoribbons, Phys. E: Low-Dimensional Syst. Nanostructures 139 (2022) 115146.

[15] Bikash Mandal, Sunandan Sarkar, Anup Pramanik, Pranab Sarkar, Doped defective graphene nanoribbons: a new class of materials with novel spin filtering properties, RSC Adv. 4 (91) (2014) 49946–49952.

[16] Lin Du, Tam N. Nguyen, Ari Gilman, André R. Muniz, Dimitrios Maroudas, Tuning the band structure of graphene nanoribbons through defect-interaction-driven edge patterning, Phys. Rev. B 96 (24) (2017) 245422.

[17] I Nikiforov, B Hourahine, Th Frauenheim, T Dumitrică, Formation of helices in graphene nanoribbons under torsion, J. Phys. Chem. Lett. 5 (23) (2014) 4083–4087.

[18] Alexandre F. Fonseca, Twisting or untwisting graphene twisted nanoribbons without rotation, Phys. Rev. B 104 (4) (2021) 045401.

[19] Alexandre F. Fonseca, Luiz Felipe C. Pereira, Length and torsion dependence of thermal conductivity in twisted graphene nanoribbons, Phys. Rev. Mater. 8 (2024) 084001.

[20] Rajesh Thakur, P.K. Ahluwalia, Ashok Kumar, Brij Mohan, Raman Sharma, Electronic structure and carrier mobilities of twisted graphene helix, Phys. E: Low-Dimensional Syst. Nanostructures 124 (2020) 114280.

[21] Alireza Shahabi, Hailong Wang, Moneesh Upmanyu, Shaping van der waals nanoribbons via torsional constraints: scrolls, folds and supercoils, Sci. Rep. 4 (2014) 7004.

[22] M. Saiz-Bretín, F. Domínguez-Adame, A.V. Malyshev, Twisted graphene nanoribbons as nonlinear nanoelectronic devices, Carbon 149 (2019) 587–593.

[23] Te-Hua Fang, Win-Jin Chang, Yu-Lun Feng, Deng-Maw Lu, Torsional characteristics of graphene nanoribbons encapsulated in single-walled carbon nanotubes, Phys. E: Low-Dimensional Syst. Nanostructures 83 (2016) 263–267.

[24] O.O. Kit, T. Tallinen, L. Mahadevan, J. Timonen, P. Koskinen, Twisting graphene nanoribbons into carbon nanotubes, Phys. Rev. B 85 (8) (2012) 085428.

[25] Kyle Rego, Vincent Meunier, Carbon nanotube knots, AIP Adv. 9 (2) (2019) 025030.

[26] Federico Bosia, Emiliano Lepore, Noe T. Alvarez, Peter Miller, Vesselin Shanov, Nicola M. Pugno, Knotted synthetic polymer or carbon nanotube microfibres with enhanced toughness, up to 1400 j/g, Carbon 102 (2016) 116–125.

[27] Nicola M. Pugno, The "egg of columbus" for making the world's toughest fibres., Plos One 9 (4) (2014) e93079.

[28] Changsheng Xiang, Colin C Young, Xuan Wang, Zheng Yan, Chi-Chau Hwang, Gabriel Cerioti, Jian Lin, Junichiro Kono, Matteo Pasquali, James M Tour, Large flake graphene oxide fibers with unconventional 100% knot efficiency and highly aligned small flake graphene oxide fibers, Adv. Mater. 25 (33) (2013) 4592–4597.

[29] Maria F. Pantano, Alice Berardo, Nicola M. Pugno, Tightening slip knots in raw and degummed silk to increase toughness without losing strength., Sci. Rep. 6 (2016) 18222.

[30] R. Kagimura, M.S.C. Mazzoni, H. Chacham, Knots in a graphene nanoribbon, Phys. Rev. B 85 (12) (2012) 125415.

[31] Shuyue Shan, Zhongwei Zhang, Shuang Lu, Sebastian Volz, Jie Chen, Generation of interfacial phonon modes and their contribution to thermal transport across the gan/ZnO interface, Phys. Rev. B 112 (2025) 155302.

[32] Weijun Ren, Shuang Lu, Cuiqian Yu, Jia He, Zhongwei Zhang, Jie Chen, Gang Zhang, Impact of moiré superlattice on atomic stress and thermal transport in van der waals heterostructures, Appl. Phys. Rev. 10 (4) (2023) 041404.

[33] William Humphrey, Andrew Dalke, Klaus Schulten, VMD: Visual molecular dynamics, J. Mol. Graph. 14 (1) (1996) 33–38.

[34] Steve Plimpton, Fast parallel algorithms for short-range molecular dynamics, J. Comput. Phys. 117 (1) (1995) 1–19.

[35] Steven J. Stuart, Alan B. Tutein, Judith A. Harrison, A reactive potential for hydrocarbons with intermolecular interactions, J. Chem. Phys. 112 (14) (2000) 6472–6486.

[36] LD.A.B. Lindsay, D.A. Broido, Optimized tersoff and brenner empirical potential parameters for lattice dynamics and phonon thermal transport in carbon nanotubes and graphene, Phys. Rev. B—Condensed Matter Mater. Phys. 81 (20) (2010) 205441.

[37] Hossein Nejat Pishkenari, Pooriya Scheel, Vibrational properties of C60: A comparison among different inter-atomic potentials, Comput. Mater. Sci. 122 (2016) 38–45.

[38] Xiangfan Xu, Luiz F C Pereira, Yu Wang, Jing Wu, Kaiwen Zhang, Xiangming Zhao, Sukang Bae, Cong Tinh Bui, Rongguo Xie, John T L Thong, Byung Hee Hong, Kian Ping Loh, Davide Donadio, Baowen Li, Barbaros Özyilmaz, Length-dependent thermal conductivity in suspended single-layer graphene, Nat. Commun. 5 (2014) 3689.

[39] Zheyong Fan, Luiz Felipe C. Pereira, Petri Hirvonen, Mikko M. Ervasti, Ken R. Elder, Davide Donadio, Tapio Ala-Nissila, Ari Harju, Thermal conductivity decomposition in two-dimensional materials: Application to graphene, Phys. Rev. B 95 (14) (2017) 144309.

[40] Florian Müller-Plathe, A simple nonequilibrium molecular dynamics method for calculating the thermal conductivity, J. Chem. Phys. 106 (14) (1997) 6082–6085.

[41] Isaac M Felix, Raphael M Tromer, Leonardo D Machado, Douglas S Galvão, Luiz A Ribeiro, Marcelo L Pereira, Irida-graphene phonon thermal transport via non-equilibrium molecular dynamics simulations, Nanoscale 16 (35) (2024) 16430–16438.

[42] Isaac M Felix, Raphael M Tromer, Leonardo D Machado, Douglas S Galvão, Luiz A Ribeiro Jr., Marcelo L Pereira Jr., Lattice thermal conductivity of 8-16-4 (sun)-graphyne from reverse nonequilibrium molecular dynamics simulations, Int. J. Heat Mass Transfer 241 (2025) 126746.

[43] Alexander Stukowski, Visualization and analysis of atomistic simulation data with OVITO–the open visualization tool, Modelling Simul. Mater. Sci. Eng. 18 (1) (2010) 015012.

[44] Gerald L. Pollack, Kapitza resistance, Rev. Modern Phys. 41 (1) (1969) 48–81.

[45] Yan Wang, Ajit Vallabhaneni, Jiuning Hu, Bo Qiu, Yong P Chen, Xiulin Ruan, Phonon lateral confinement enables thermal rectification in asymmetric single-material nanostructures., Nano Lett. 14 (2) (2014) 592–596.

[46] Leonardo Medrano Sandonas, Rafael Gutierrez, Arezoo Dianat, Giovanni Cuniberti, Engineering thermal rectification in MoS2 nanoribbons: a non-equilibrium molecular dynamics study, RSC Adv. 5 (67) (2015) 54345–54351.

[47] Zheyong Fan, Petri Hirvonen, Luiz Felipe C Pereira, Mikko M Ervasti, Ken R Elder, Davide Donadio, Ari Harju, Tapio Ala-Nissila, Bimodal grain-size scaling of thermal transport in polycrystalline graphene from large-scale molecular dynamics simulations., Nano Lett. 17 (10) (2017) 5919–5924.

[48] Yang Kang, Fuyan Duan, Shaoxin Shangguan, Yixin Zhang, Tianpei Zhou, Bingcheng Si, Thermal transport of graphene sheets with fractal defects., Mol. (Basel, Switzerland) 23 (12) (2018).

[49] Alexey N. Volkov, Takuma Shiga, David Nicholson, Junichiro Shiomi, Leonid V. Zhigilei, Effect of bending buckling of carbon nanotubes on thermal conductivity of carbon nanotube materials, J. Appl. Phys. 111 (5) (2012) 053501.

[50] Zhengxing Huang, Zhen'an Tang, Jun Yu, Suyuan Bai, Temperature-dependent thermal conductivity of bent carbon nanotubes by molecular dynamics simulation, J. Appl. Phys. 109 (10) (2011) 104316.

[51] Fumio Nishimura, Takuma Shiga, Shigeo Maruyama, Kazuyuki Watanabe, Junichiro Shiomi, Thermal conductance of buckled carbon nanotubes, Japan. J. Appl. Phys. 51 (1) (2012) 015102.

[52] Victor Lee, Renkun Chen, Chih-Wei Chang, Probing the limit of one-dimensional heat transfer under extreme bending strain, Phys. Rev. B 87 (3) (2013) 035406.

[53] C.W. Chang, D. Okawa, H. Garcia, A. Majumdar, A. Zettl, Nanotube phonon waveguide., Phys. Rev. Lett. 99 (4) (2007) 045901.

[54] Jihong Al-Ghalith, Traian Dumitrică, Nano-scale heat transfer in nanostructures: Toward understanding and engineering thermal transport, Springer Briefs in Applied Sciences and Technology: Thermal Engineering and Applied Science, Springer International Publishing, Cham, 2018.

[55] Philip B. Allen, Size effects in thermal conduction by phonons, Phys. Rev. B 90 (5) (2014) 054301.

[56] Andrea Cepellotti, Nicola Marzari, Boltzmann transport in nanostructures as a friction effect., Nano Lett. 17 (8) (2017) 4675–4682.

[57] Fergany Badry, Karim Ahmed, A new model for the effective thermal conductivity of polycrystalline solids, AIP Adv. 10 (10) (2020) 105021.

[58] Shiqian Hu, Zhongwei Zhang, Pengfei Jiang, Weijun Ren, Cuiqian Yu, Junichiro Shiomi, Jie Chen, Disorder limits the coherent phonon transport in two-dimensional phononic crystal structures, "Nanoscale" 11 (2019) 11839–11846.

[59] Xavier Cartoixà, Luciano Colombo, Riccardo Rurali, Thermal rectification by design in telescopic si nanowires., Nano Lett. 15 (12) (2015) 8255–8259.

[60] Haidong Wang, Shiqian Hu, Koji Takahashi, Xing Zhang, Hiroshi Takamatsu, Jie Chen, Experimental study of thermal rectification in suspended monolayer graphene., Nat. Commun. 8 (2017) 15843.

[61] Xiao Yang, Xinghua Zheng, Qiushi Liu, Ting Zhang, Ye Bai, Zheng Yang, Haisheng Chen, Ming Liu, Experimental study on thermal conductivity and rectification in suspended monolayer mos2., ACS Appl. Mater. Interfaces 12 (25) (2020) 28306–28312.

[62] Fayong Liu, Manoharan Muruganathan, Yu Feng, Shinichi Ogawa, Yukinori Morita, Chunmeng Liu, Jiayu Guo, Marek Schmidt, Hiroshi Mizuta, Thermal rectification on asymmetric suspended graphene nanomesh devices, Nano Futur. 5 (4) (2021) 045002.

[63] Oliver Gröning, Shiyong Wang, Xuelin Yao, Carlo A Pignedoli, Gabriela Borin Barin, Colin Daniels, Andrew Cupo, Vincent Meunier, Xinliang Feng, Akimitsu Narita, et al., Engineering of robust topological quantum phases in graphene nanoribbons, Nature 560 (7717) (2018) 209–213.

[64] Widianto P. Moestopo, Sammy Shaker, Weiting Deng, Julia R. Greer, Knots are not for naught: Design, properties, and topology of hierarchical intertwined microarchitected materials, Sci. Adv. 9 (10) (2023) eade6725.

[65] Rajesh Kumar Sharma, Ishita Agrawal, Liang Dai, Patrick Doyle, Slaven Garaj, DNA knot malleability in single-digit nanopores, Nano Lett. 21 (9) (2021) 3772–3779, PMID: 33661654.

[66] Xiangfan Xu, Luiz F.C. Pereira, Yu Wang, Jing Wu, Kaiwen Zhang, Xiangming Zhao, Sukang Bae, Cong Tinh Bui, Rongguo Xie, John T.L. Thong, Byung Hee Hong, Kian Ping Loh, Davide Donadio, Baowen Li, Barbaros Özyilmaz, Length-dependent thermal conductivity in suspended single-layer graphene, Nat. Commun. 5 (1) (2014) 3689.